Development of Rhombus Hanging Basket Walking Track Robot for Cantilever Casting The construction in Bridges

Yuping Ouyang *, Jiarui Huang, Kaifang Song

Posted Date: 26 July 2023

doi: 10.20944/preprints202307.1758.v1

Keywords: Cantilever the construction; Rhombus hanging basket; Walking track; Finite element simulation; Mechanical characteristics

Article

Development of Rhombus Hanging Basket Walking Track Robot for Cantilever Casting The Construction in Bridges

Yuping Ouyang [1,2,*], Jiarui Huang [1,2] and Kaifang Song [1,2]

[1] School of Mechanical and Electrical and Vehicle Engineering, East China Jiaotong University, Nanchang 330013, China.
[2] National and Local Joint Engineering Research Center for Fruit Intelligent Photoelectric Detection Technology and Equipment, Nanchang 330013, China
* Correspondence: ouyuping1987@163.com

Abstract. For enhancing the efficiency of cantilever casting the construction in the bridge, a novel rhombus traveling track of hanging basket was developed and optimized. The civil software titled Midas was applied to analyse the mechanical properties of the hanging basket with full load and control load. The strength and distortion of the walking mechanism were within the specified range when the maximum beam unit internal force of 149.69Mpa, which was less than the allowable stress of steel 175Mpa, and the anti-overturning safety factor of the hanging basket was 2.5 to meet the requirements. Through the comparative analysis of the key components and the finite element calculation, it was found that there was about 30% redundancy in the structure performance. Therefore, further optimization of each structure was carried out, and the front elevation of the main truss of 20° was achieved. It obtained the best performance in all aspects.

Keywords: cantilever the construction; rhombus hanging basket; walking track; finite element simulation; mechanical characteristics

1. Introduction

The cantilever pouring the construction method of the bridge was one of the most important methods to solve the construction problems of river crossing bridge. The rhombic hanging basket had stable structure, high utilization efficiency, convenient disassembly, movement, so it was most widely used in cantilever the construction (Hyo and Je, 2004; Won et al., 2008); the method generally adopted the hanging basket the construction technology. The hanging basket can bear the load and beam weight in the construction process. It was designed without a unified, systematic and perfect standard. Hence, before the application of the hanging basket, a reasonable design and accurate mechanical checking calculation can be carried out to ensure its safety in the construction process (Liu et al., 2019; Zhao et al., 2017).

In the meantime, domestic and foreign scholars have carried out relevant research (Mashal and Palermo, 2019; Li et al., 2020). Li (2018) used a prestressed concrete continuous beam bridge as a support during the the construction of the Mao-ji-te Bridge and introduced the differences due to the difference in the load-bearing structure. Four types of hanging baskets were listed. The main structure and force characteristics of different structural types of hanging baskets were analysed in detail. In addition, the different characteristics of specific projects were combined to select the hanging basket structure suitable for the actual project (Li, 2018). Gao (2016) shortened the length of the hanging basket by setting a triangular truss on the cast-in-place main beam. He combined the advantages of the front fulcrum hanging basket and the middle fulcrum hanging basket and proposed a short platform composite traction rope hanging basket to improve the problem that the main beam section can be changed when the long platform traction rope hanging basket walked (Gao, 2016); the above studies were the introduction of different hanging basket structures during cantilever beam pouring and summarized the matters needing attention to ensure the safe the

 doi:10.20944/preprints202307.1758.v1

construction of hanging basket. However, there was still a lack of finite element modeling analysis and discussion on hanging basket the construction and walking. Chen et al. (2013) described the key points of the main truss of the triangular hanging basket in the design process and carried out spatial modeling, analysis and calculation of the structure through MIDAS / civil program, which put forward theoretical support for the finite element simulation of cantilever hanging basket the construction in the future (Chen, 2013); An et al. (2018) proposed that the high pier long-span continuous rigid frame aqueduct in Xujiawan was constructed by cantilever method, and the first-order method of ANSYS was used for optimization calculation (An, 2018). The original rhombic hanging basket was transformed. Apart from these, a cable-stayed combined light rhombic hanging basket combining the traditional rhombic hanging basket and the sliding cable-stayed hanging basket was raised, which reduced the quality of the hanging basket and improved the utilization coefficient; Gu et al. (2019) added the transportation system and hoisting system to the traditional hanging basket structure. After the corrugated steel web was lifted to the poured beam surface, the transportation system moved it to the hanging basket hoisting starting point (Gu, 2019). And then the corrugated steel web was installed through the hoisting system. The feasibility of the composite structure was verified through calculation and finite element simulation; in order to overcome the shortcomings of traditional balanced cantilever the construction, He et al. (2020) introduced a new asynchronous pouring the construction technology. It made full use of the excellent shear resistance of corrugated steel webs to support the hanging basket, optimized the walking system, increased the construction platform, effectively accelerated the the construction speed, reduced the construction load, and saved the project cost (He et al., 2020); Zhou et al. (2020) combined with the excellent shearing capacity of the corrugated steel mesh and introduced asynchronous pouring and rapid the construction methods. A significant change was that it used the corrugated steel mesh itself as the main load-bearing member to support the hanging basket and beam sections. In the new method, the balance state of the new hanging basket system was optimized from the cantilever to the pure support state, and the walking system was optimized in the meantime, which greatly shortened the construction time and ensured the safety of the project (Zhou et al., 2020).

Generally speaking, the research so far has mainly focused on the optimization and transformation of the main truss structure of the cradle. The shortcomings of the walking system of the cradle still existed, and there were few studies in this area. Relevant industrial standards have not yet been established and were difficult to be set up in hanging basket-related equipment. Consequently, it is indispensable to calculate and simulate the mechanical properties of different equipment in order to ensure the safety of the construction process. Relying on the Tianjin Haihe Bridge project, this paper proposed a new type of traveling rail for the cradle and optimized the structure of the main truss of the rhombus cradle, which solved the problem of low efficiency in the construction of the traditional cradle. Through calculation and finite element simulation, the hanging basket met the engineering requirements.

2. Material and Methods

This section introduced the project overview of Tianjin Hai-he River Bridge. In view of the shortcomings in the past bridge the construction process, a basket walking track with simple walking mode and lighter weight was designed to be used in the Hai-he River Bridge project. The track was made of a new type of polymer. The manufacturing process of the track and materials was introduced, and the track was modeled. The mechanical properties of the track materials were tested according to the Chinese national standards. The structure of the hanging basket was introduced and modeled, and different working conditions in the construction were designed. In order to verify the reliability of the rails and cradles made of new polymer materials used in practical projects, according to the models of the cradles and tracks established in the previous model, Abaqus and Midas/civil software were used to simulate and analyze the rails and cradles, analyze the stability of the rails and cradles, and make the structures met the safety requirements in the project.

Preprints (www.preprints.org) | NOT PEER-REVIEWED | Posted: 26 July 2023 doi:10.20944/preprints202307.1758.v1

2.1. Project Profile

The Hai-he Bridge was an extra-large bridge in the southern section of the Tang-Jin Expressway Expansion Project. It was designed to cross Tian-jin Hai-he River and the total length was 2850m. The main bridge was a three-span continuous girder structure with a span combination of (100+160+100)m. As shown in Figure 1, it is the longitudinal section. The The height of main pier was 19.5m, and the upper part of the main bridge adopted a prestressed concrete continuous box girder. The section was a single box and single cell with straight webs. As shown in Figure 2, it was the cross section of the suspended cast block. The beam height of the fulcrum of the main span, the beam height of the middle span, the top width of the single box beam, the bottom plate width, and the box beam flange width were 9.5m, 3.5m, 13.25m, 6.25m and 3.5m. And the beam height changed according to 1.8 times parabola. There were 18 suspended cast blocks in total, of which block 9 was the heaviest, with a concrete volume of 79.3 m^3, a weight of 206.96t, and a length of 4.5m.

Figure 1. The longitudinal section of the main bridge.

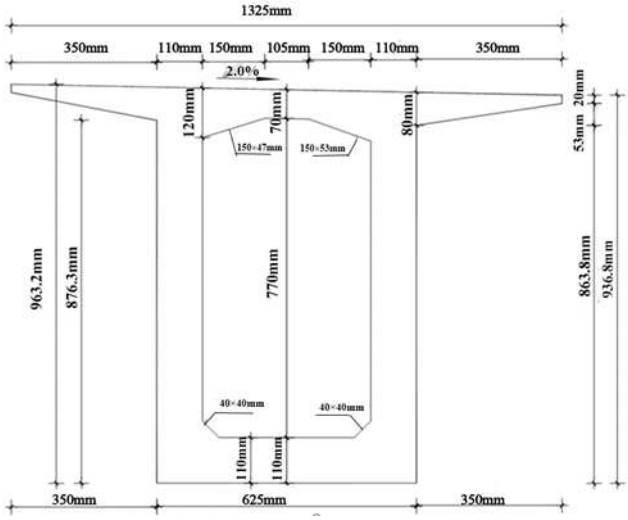

Figure 2. Cross section of suspended pouring block.

2.2. Structure of Rhombus Rraveling Track of Hanging Basket

2.2.1. Structure of Walking Track

A. Introduction to the Structure of Walking Track

The track height and center of gravity of the traditional hanging basket walking mechanism were high, which were increasing the risk of the hanging basket overturning (Xie et al., 2017). Simultaneously, the walking track was long and bulky, and the laying and dismantling process was complex, which limited the improvement of engineering efficiency (Somaini and Furst, 2020). Based on the above problems, a new-type walking track of the hanging basket was designed, which was light and easy to be disassembled and assembled. Its single-chip chain plate structure was shown in Figure 3.

Preprints (www.preprints.org) | NOT PEER-REVIEWED | Posted: 26 July 2023 doi:10.20944/preprints202307.1758.v1

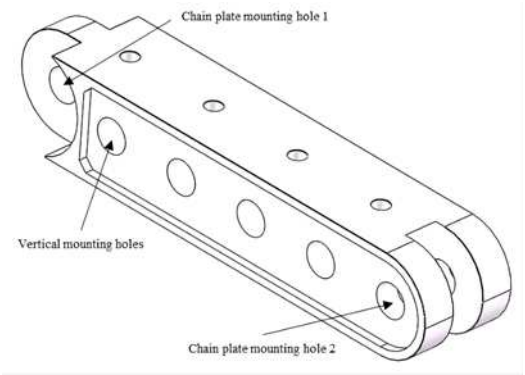

Figure 3. New type of walking track chain plate structure.

B. Preparation of Walking Track

The material preparation equipment of the new-type hanging baskets walking track was a twin-screw extrude, as shown on the left side of Figure 4. The preparation method was to add 3% of SWR-3F nylon toughening agent, 2% of 2-Hydroxybenzophenone, 3% of organic phosphate, and 50% of PA6 chips in the mixing bucket of Figure 4 according to the mass ratio. After mixing, uniformly, put it into the extrude through the hopper, heat it and feed the material in the middle of the extrude. According to the mass ratio, add 15% of LEE powder, 5% of KH550 coupling agent, and 22% of glass fiber. And vacuumize, heat all the materials in the extrude to 260℃, and enter the cooling pool to cool after molding, then shear and granulate into fine particles, as shown on the right side of Figure 4. After that, it was passed through the single-screw extrude to heat and combined pelletizing and forming, and finally obtained the light weight material of the hanging basket. The glass fiber and ultrafine powder particle treated with coupling agent were added to improve the tensile strength of the material (Li et al., 2021; Kosobokov et al., 2020), and SWR-3F toughening agent was added to improve the impact resistance of the material (Ying et al., 2020; Wolk et al., 2018; Hu et al., 2018).

When the new hanging basket track was used, the convex part of the first chain plate was inserted into the recess part of the second chain plate, so that the chain plate mounting hole 1 of the first chain plate can be aligned with the chain plate mounting hole 2 of the second chain plate. Bolts were inserted into the aligned holes for connection. In the same measure, multiple chain plates can be connected to form load-bearing chain plate track. For the baskets of different sizes, several rows of the load-bearing chain plate tracks can be arranged side by side, so that the vertical mounting holes on the side-by-side chain plates were aligned and inserted with bolts on connection. Therefore, the bearing area of chain bearing plate tracks can be increased. In this project, each rhombic truss had four load-bearing chain plates, as shown in Figure 5. The gap between the middle load-bearing chain plate tracks served to avoid contacting the finishing steel bar on the bridge deck. The front support of the main truss of the hanging basket was installed on the walking trolley. When the hanging basket was walking, the hydraulic push rod applied force on the connecting pin fixed on the chain plate. Due to the counter-effect of force, the hydraulic push cylinder traveled away from the axis pin to complete the walking of the hanging basket equipment.

Preprints (www.preprints.org) | NOT PEER-REVIEWED | Posted: 26 July 2023 doi:10.20944/preprints202307.1758.v1

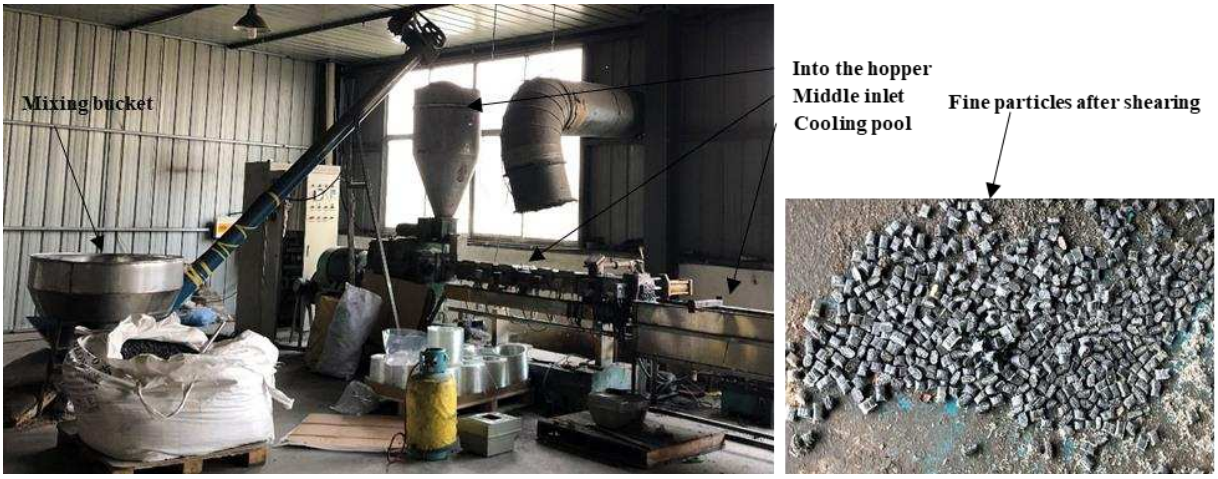

Figure 4. Twin screw extruder and granulation.

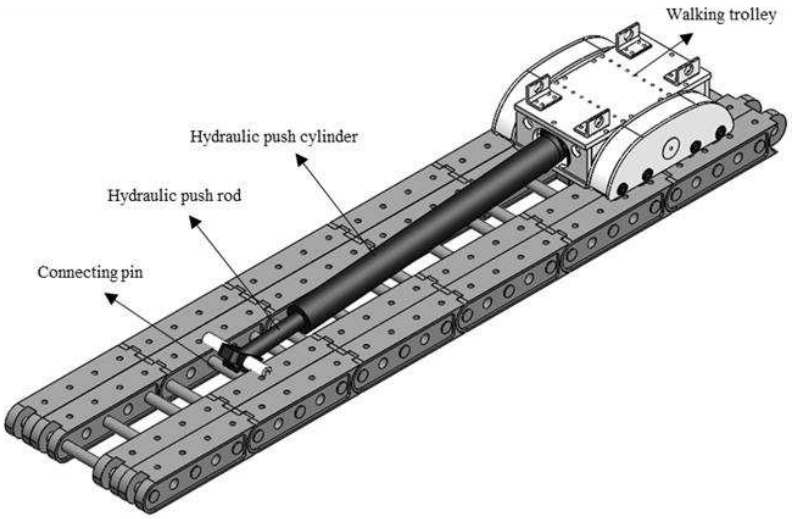

Figure 5. Load bearing chain plate track.

C. Material performance test of Walking Track

The new walking track material was consisted of 3% SWR-3F nylon toughener, 2% 2-hydroxyphenyl benzophenone, 3% phosphate ester, and 50% nylon 6 chips, 15% LEE powder, 5% KH550 coupling agent and 22% glass fiber composition. Because of the new materials used in the track, this paper tested the mechanical properties according to the Chinese national standard(GB2918). The standard requires that the test sample should be in a constant environment and the test temperature should be 18℃-28℃, and it is suitable for the mechanical property test of plastic samples. According to the actual stress condition and working environment of the hanging basket, the tensile performance, compressive performance, and impact resistance of the new materials were selected to be tested.

1. Tensile Property Test

The tensile property test schedule was shown in Table 1. Firstly, the material which was easy to be fixed by the fixture was produced according to the standard, as shown in Figure 6a. The width and thickness of the tensile part in the middle of the sample were 10 mm and 4 mm and the tensile section area was 40 mm^2 as shown in Figure 6b.

Preprints (www.preprints.org) | NOT PEER-REVIEWED | Posted: 26 July 2023 doi:10.20944/preprints202307.1758.v1

Table 1. Tensile property test schedule.

Experimental instrument	Electronic universal testing machine
Experimental temperature	20℃
Stretching speed	50mm/min
Test repetition times	5
Number of test samples	5

The device used in the experiment was an electronic universal testing machine. The test sample was in a constant environment. The test environment temperature was 20℃. The test method was as follows: Firstly, the materials tested were clamped tight according to the set gauge length, as well as the distance between the upper clamp and the lower one was 120mm, as shown in Figure 6b. Secondly, calibration and zero-setting were conducted in the software, and the tensile test was started at the speed of 50mm per minute. The experiment was terminated at the moment when the material was fractured. The experiment sample shown in Figure 6 was repeated five times. The five groups of experimental results were summarized and averaged, as shown in Figure 7. Before the point A, under the condition that the sample was not completely tightened by the clamp, the test force was relatively low and would not be enhanced during the process of trying to clamp. The sample was totally tightened by the clamp at the time of 1.30s (point A) when the test force started to increase. At the time of 9.9s (point B), the test force and stress reached the maximum, followed by a small and temporary drop; then the material was broken and the testing machine stopped loading to finish the experiment. The stress at point B served as the maximum stress of the sample, which was the tensile strength of the material with a measured value of 95.55Mpa.

Figure 6. New materials in tensile test: (**a**) Before the test (Left), (**b**) After the test (Right).

Preprints (www.preprints.org) | NOT PEER-REVIEWED | Posted: 26 July 2023 doi:10.20944/preprints202307.1758.v1

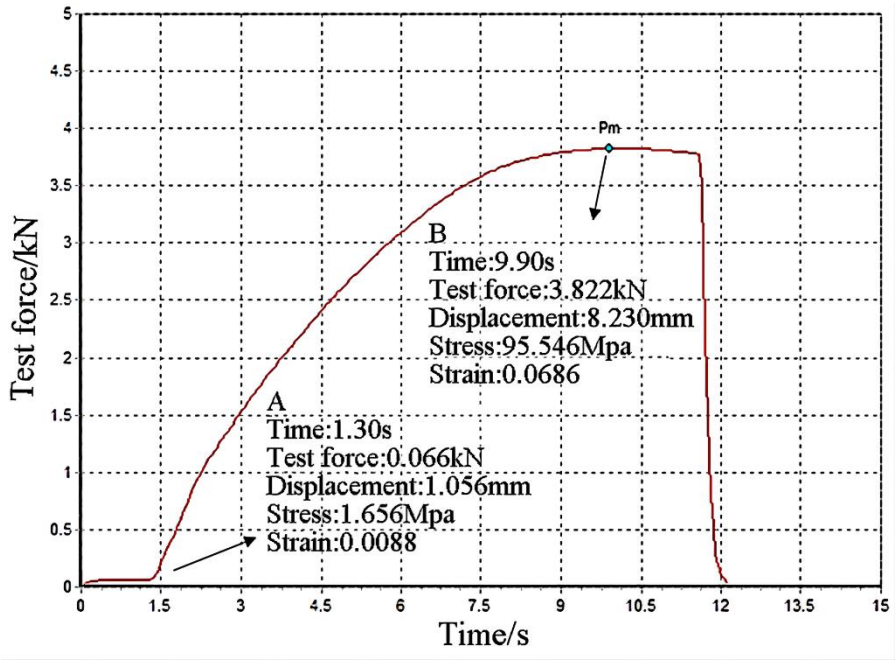

Figure 7. Time and test force curve of tensile test sample.

2. Compressive Performance Test

The tensile property test schedule was shown in Table 2. Compressive strength of the new materials needs to be tested by testing their compressive properties. The sample used for the test was shown in Figure 8. The compressive strength test applied uniform load in the direction of side A. The length and width of the sample was 10.5mm, the compression area was 110.25mm2 and the height was 30mm.

Table 2. Schedule of compression performance test.

Experimental instrument	Electronic universal testing machine
Experimental temperature	20℃
Compression speed	10mm/min
Test repetition times	5
Number of test samples	5

The instrument used in the test was an electronic universal testing machine. The test sample was in a constant environment. The test environment temperature was 20℃. The test method was as follows: Firstly, the remaining material at both ends of the sample was polished by sandpaper, and the A-side of the sample should be placed upward on the stage. Calibration and zeroing were then performed in the computer software, and the compression test was started at 10 mm/min and stopped when the sample collapsed. The experiment sample shown in Figure 8 was repeated five times. The test was repeated for 5 groups, and the sample that collapsed due to compression, as shown in Figure 9. The parameters and results of each group of tests needed to be recorded. The five groups of experimental results were summarized and averaged, as shown in Figure 10. Before the point A, the sample was not entirely compacted by the testing machine, and the stress caused by the slight unevenness of the sample surface after compaction was relatively small. From the point A, the sample was under complete stress which was increased sharply. At the beginning of point B, the increase of the stress then witnessed a downturn and reached its maximum at point C. After point C, the material

 doi:10.20944/preprints202307.1758.v1

was fractured upon the maximum stress, resulting in a drastic drop of the stress. Then the testing machine stopped loading, and the experiment came to an end. The stress at point C was the tensile strength of the sampled material with a measured value of 109.88Mpa.

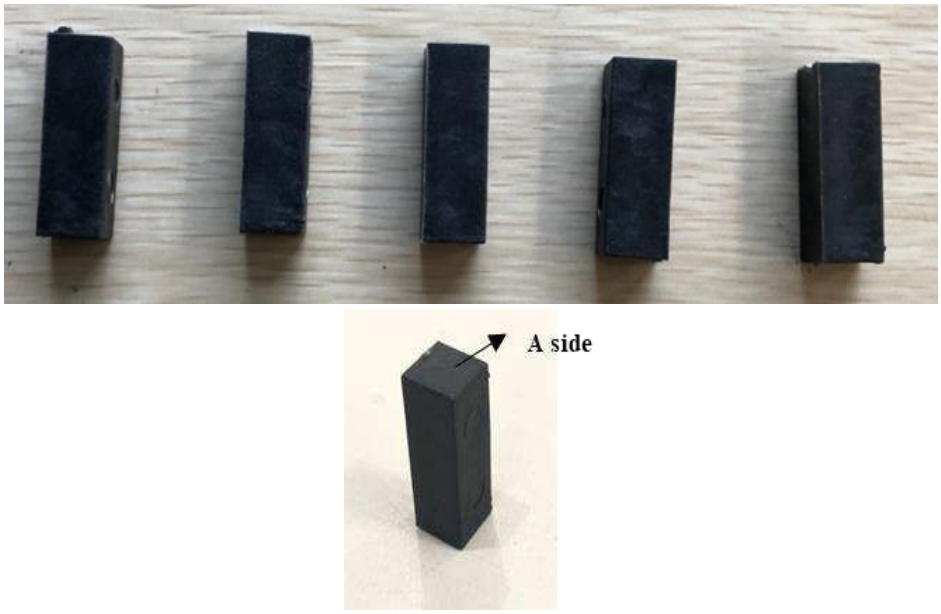

Figure 8. Compression test specimen.

Figure 9. Specimen collapsed in the compression test.

Preprints (www.preprints.org) | NOT PEER-REVIEWED | Posted: 26 July 2023 doi:10.20944/preprints202307.1758.v1

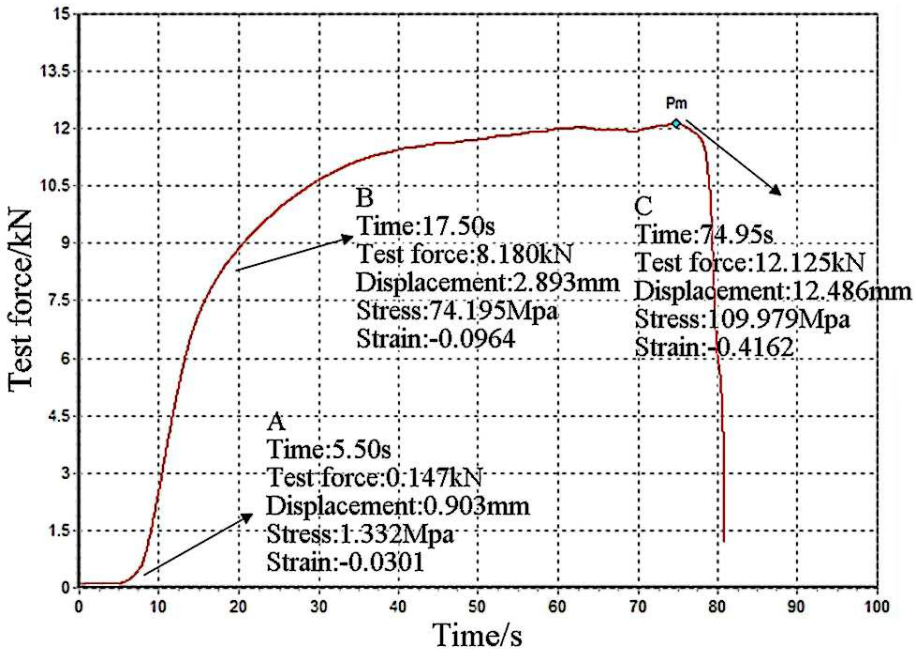

Figure 10. Time and force curve of compression test.

3. Impact Resistance Test

The tensile property test schedule was shown in Table 3. Standard size material was produced according to the standard. The length of the sample, the width and thickness were 80mm, 10mm ,and 4mm. And the cross-sectional area was 40mm^2, as shown in Figure 11.

Table 3. Impact resistance test schedule.

Experimental instrument	Impact testing machine
Experimental temperature	20℃
Pendulum energy	7.5J
Impact speed	3.8m/s
Test repetition times	5
Number of test samples	5

The instrument used in the test was an electronic simple suspension combined impact testing machine. Samples were made according to the standard, and the number of measurements was 5 groups. The test sample was in a constant environment. The test environment temperature was 20℃, and the test method was as follows: The pendulum was fixed to the upper part of the instrument. The sample was placed on the impact table. With the button of bounce pressed, the sample was broken by the falling pendulum bob, and the corresponding data was recorded by the device. The broken samples after the experiment was shown in Figure 12. The results were summarized upon the completion of the present five groups of experiments. As shown in the table, the "angle of elevation" referred to the angle between the originally fixed position of the pendulum and the vertical line; The "air attack angle" referred to the calculated angle at which the pendulum rotated in the air after deducting the thickness of the material; The "impact angle" referred to the angle between the highest point reached on the other side after pendulum broke the sample and the vertical line. It was analyzed that the smaller the impact angle was, the larger the impact strength of the material was. The

Preprints (www.preprints.org) | NOT PEER-REVIEWED | Posted: 26 July 2023 doi:10.20944/preprints202307.1758.v1

calculation of the impact strength a_{cU} of the specimen was shown in Equation (1), where E_{cU} was the energy absorbed by the measured pattern. The experiment sample shown in Figure 11 was repeated five times. The five groups of experimental results were summarized and averaged, as shown in Table 4. It can be seen from Table 4 that the impact angle of test group 4 was larger because the material was not uniform in the molding process, resulting in a thicker position in the middle and more materials, so the impact strength was increased slightly. The impact strength of the material was 67.65 kJ / m².

$$a_{cU} = \frac{E_{cU}}{h_{cU} b_{cU}} \times 10^3 \quad (1)$$

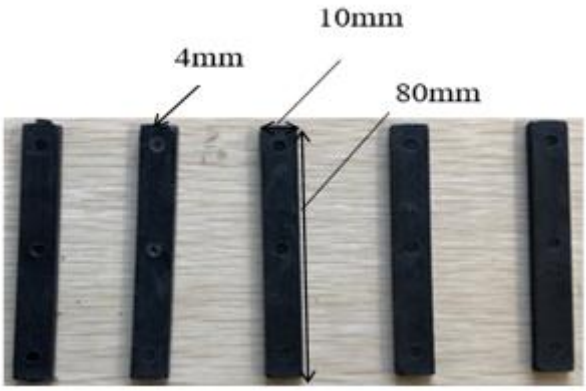

Figure 11. New material in impact resistance test.

Figure 12. Sample broken after test.

Table 4. Summary of impact test results.

Experiment	Elevation [°]	Air attack angle[°]	Impact angle[°]	Absorbed energy[J]	Impact strength [kJ/m²]
1	160	158.40	101.92	2.797	69.92
2	160	158.40	103.63	2.685	67.12
3	160	158.40	107.23	2.452	61.30
4	160	158.40	98.55	3.022	75.55
5	160	158.40	105.36	2.575	64.37

2.2.2. Structure of Hanging Basket

A. Introduction to the structure of the Hanging Basket

Cantilever casting rhombic hanging basket was adopted in constructing the main span of this project. The basket was mainly composed of 2 rhombic main trusses and connecting parts, which constituted the main load-bearing system, bottom basket, suspension system, rear anchor, walking system, and formwork system. The transverse distance between the two rhombic main trusses was

Preprints (www.preprints.org) | NOT PEER-REVIEWED | Posted: 26 July 2023 doi:10.20944/preprints202307.1758.v1

5.7m. The upper and lower chords of the main truss were consisted of □400×300×12mm rectangular steel pipe, while the vertical web member was made of □350×250×10mm rectangular steel pipe; the front tilt web member under compression was composed of □400×300×12mm rectangular steel tubes, the rear tilt web member under compression was consisted of □420×300×12mm grooved steel, and the casing pipe guide beam of the lower chord was made of □350×250×12mm rectangular steel pipe; The upper beam was composed of a double-split □200×400×10mm rectangular steel pipe, the front and rear beams of the bottom basket were consisted of □400×300×12mm rectangular steel pipe, and the longitudinal beam of the bottom basket was made of HN150×300×6.5×9-6000mm H-type steel; The hanger was consisted of double Φ32 fin twisted steel bar. The transverse door union was made of the square steel tubular truss with a vertical height of 1400mm and a transverse width of 500mm. The chord was consisted of □120×120×5mm steel pipe, and the web member was composed of □100×50×4mm steel pipe; the outer guide beam was made of 350×250×12mm rectangular steel tube, and the main structural steel materials of the hanging basket were Q235 steel. The structure diagram of the main truss was shown in Figure 13.

The weight of the hanging basket was 63t. In the worst case, the total weight of the formwork was 22.8t. The static load coefficient and dynamic load coefficient of the hanging basket were 1.2 and 1.4 respectively. In the running process of the hanging basket, the two most typical working conditions were selected for analysis, whose wind speed was both 13.6m/s vertically downward. Among them, working condition 1 referred to the the construction process of segment 9 (with the heaviest pouring concrete); Working condition 2 referred to the hanging basket of walking state.

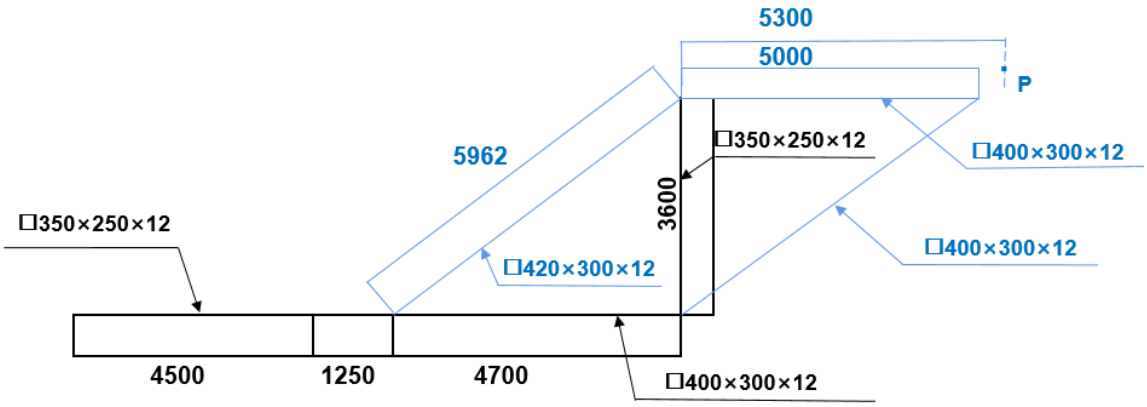

Figure 13. Dimensions of the main truss.

B. The construction of Finite Element Model of the Hanging Basket

Firstly, a three-dimensional model was established in SolidWorks software according to the entity of the cradle. According to the established three-dimensional diagram, the model was imported into MIDAS / civil software to establish the finite element simulation model of the cradle, as shown in Figure 14.

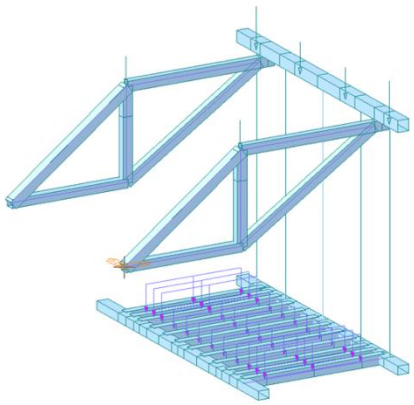

Preprints (www.preprints.org) | NOT PEER-REVIEWED | Posted: 26 July 2023 doi:10.20944/preprints202307.1758.v1

Figure 14. Overall calculation model of hanging basket.

According to the force transfer characteristics and load transfer mechanism of the member connection in the structure, it was found that the boundary conditions of the structure mainly included the main truss system boundary condition and the suspension boundary condition. The main truss was completely fixed on the traveling track and cannot be moved. Therefore, the displacement needed to be fully constrained and the rotation was not constrained. The suspension boundary condition was the relationship between the suspender connecting the upper beam and the lower beam. The two nodes of the front upper beam and the main truss were connected elastically to play the role of suspending the bottom basket and pouring the concrete load.

C. Working condition of the Hanging Basket

This paper was divided into the following three conditions for analysis and calculation. The wind direction of the three conditions was vertical downward (wind speed 13.6m/s). Condition 1 and condition 2 was calculated by MIDAS / civil, and condition 3 was calculated by referring to the Chinese national standard. In condition 1, the hanging basket was located at the 9 # section, which was the heaviest section of 4m, and the weight of pouring concrete was 125t. When the concrete pouring was completed but not solidified, the stress and distortion of the hanging basket in the working state were calculated; in condition 2, the hanging basket walked to the end of the newly poured section, and did not mount the concrete itself. In condition 3, the hanging basket was in the walking state, and the stability of the hanging basket in the working state was calculated.

2.3. Simulation of the Walking Track and the Hanging Basket

2.3.1. Finite Element Simulation of New Material for Walking Track

According to Chinese national standards, the above experimental results of the new material of the cradle track demonstrated that the structure had high tensile strength, high compressive strength and good impact resistance. In the meantime, finite element simulations have been carried out to verify its reliability in practical engineering application. In order to verify the reliability of the hanging basket track chain plate made of new polymer materials in practical engineering, the model of single track chain plate would be established in solidworks software. Because Abaqus software can simulate the properties of engineering materials, the model would be imported to Abaqus for simulation.

The track of the hanging basket was paved on the surface of the bridge, on which the main truss carrying the to-be-cast concrete was walking and moving. Firstly, the boundary conditions for the simulation were set to constraint the freedom degree of the bottom surface of the model(without other structural support). The track chain plates were installed embedded into each other, so there were some missing material positions under the surface of a single chain plate, as shown in the point A of Figure 15. Therefore, for convenient calculation, the bearing area of the hanging basket track was reduced without calculating the place where the material was missing, and the evenly distributed load was applied to the effective areas. The calculation was done under the condition of the maximum bearing capacity of 8 tracks operating. In addition, the safety coefficient and the evenly distributed load stood at 1.1 and 142.39t respectively, as shown in Figure 16.

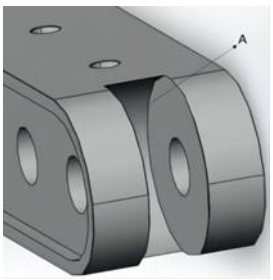

Preprints (www.preprints.org) | NOT PEER-REVIEWED | Posted: 26 July 2023 doi:10.20944/preprints202307.1758.v1

Figure 15. Missing points of internal material.

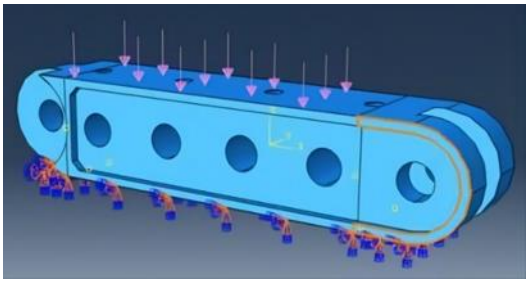

Figure 16. Boundary conditions and uniform load of chain plate.

From the simulation results shown in Figure 17, the position of the overall stress distribution of the track where the stress changed the most was on both sides of the surface of the hole position. The maximum stress was 122Mpa, which was greater than 110Mpa. Thus, the simulation results proved that the track chain plate made of the new material can be applied in the the construction process of the hanging basket.

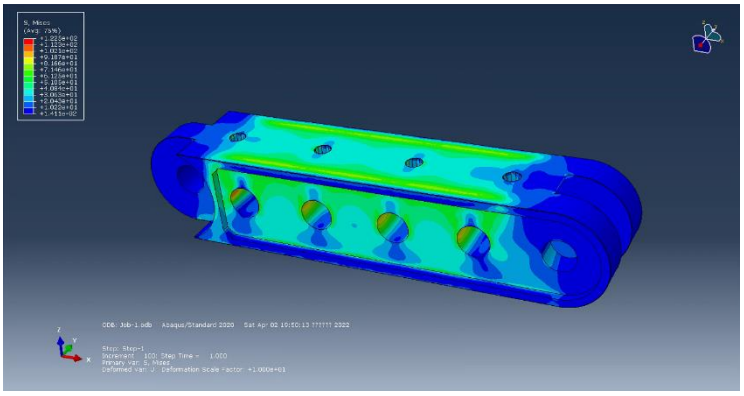

Figure 17. Mechanical simulation results.

2.3.2. Finite Element Simulation of the Hanging Basket Structure Based on Midas/Civil

Due to the convenience of Midas software, the model of the hanging basket was established in Midas/Civil software. The load was applied to calculate the stress and distortion of the hanging basket under the condition of No.9 section the construction (the heaviest pouring concrete) in condition 1. The overall calculation model of the hanging basket was shown in Figure 14. In the cantilever casting the construction, the hanging basket equipment was generally divided into three states in Section 2.2.2(C) above. The combined load analysis was adopted.

A. Analysis on Mechanical Performance of the Hanging Basket under Condition 1

Apply the above finite element model, apply the load, analyze and calculate the deformation and stress of the structure. From Figures 18 and 19, the calculated stress cloud diagram and vertical distortion cloud diagram of hanging basket structure can be seen, respectively. As can be seen from Figure 18, the vertical distortion of 12.53mm occurred at the upper end of the main truss, which was less than 1/400 of the length of the member(13.25mm); the vertical displacement of 25.00mm occurred in the middle of the front upper beam, which was 12.47mm, which was less than 1/400 of the length of the member(30mm) due to the reference system; The vertical displacement of 28.65mm occurred in the middle of the front lower beam, which was 16.12mm. The distortion of the structure met the design requirements.

As can be seen from Figure 19, the maximum beam unit internal force generated by the whole structure was 149.69Mpa, which occurred at the junction of the front upper beam and the main truss.

Preprints (www.preprints.org) | NOT PEER-REVIEWED | Posted: 26 July 2023 doi:10.20944/preprints202307.1758.v1

The stress of the structure was less than the allowable stress of Q235 steel $\left[\sigma_{Q235}^{\alpha}\right]=175\,MPa$ (Wu et al., 2018), which met the design requirements of the project. In addition, it was indispensable to analyse the main components of the hanging basket.

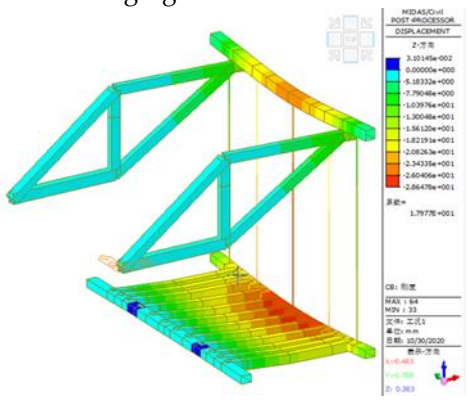

Figure 18. Z-direction distortion nephogram of the whole structure of the hanging basket under condition 1.

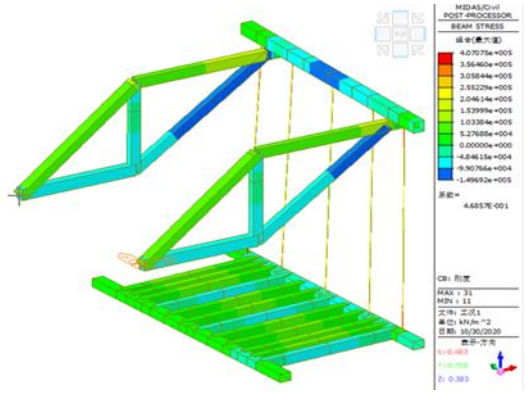

Figure 19. Stress nephogram of overall structure of hanging basket under condition 1.

1. Main Truss

The main truss was the main load-bearing member(Zhou et al., 2014), which was composed of upper and lower chords(AB,CD), vertical web members(BD), tension diagonal web members(AD) and compression diagonal web members(BC), all of which were made of Q235. According to the finite element analysis results of Figures 20 and 21, the maximum distortion and maximum stress at the front end of the main truss were 12.53mm and 149.69Mpa respectively. The analysis summary of the maximum stress, axial force and distortion of each member of the main truss were shown in Table 5. Each member of the main truss met the design requirements of the project.

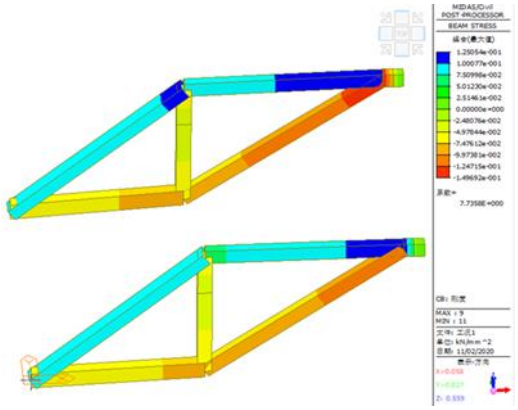

Preprints (www.preprints.org) | NOT PEER-REVIEWED | Posted: 26 July 2023 doi:10.20944/preprints202307.1758.v1

Figure 20. Distortion nephogram of main truss structure under condition 1.

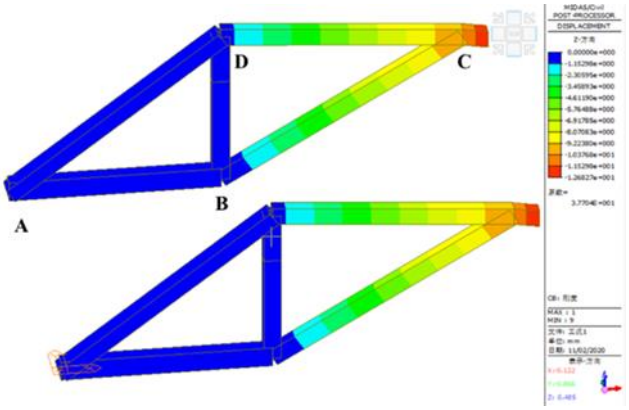

Figure 21. Stress nephogram of main truss structure under condition 1.

Table 5. Analysis of each member of main truss under condition 1.

Member name	Max stress [Mpa]	Max vertical distortion [mm]	Allowable stress [Mpa]	Allowable distortion [mm]
AB	92.6	0.25	175	11.75
CD	149.7	12.53	175	13.25
BD	55.0	0.41	175	9.00
AD	103.9	0.60	175	14.91
BC	134.2	10.33	175	15.25

2. Front Upper Crossbeam

The front upper crossbeam was fixed at both ends of the upper chord of the main truss. According to the finite element analysis results from Figures 22 and 23, the maximum distortion in the middle of the front upper crossbeam was 25.00mm. Due to the reference system, the actual maximum distortion and the maximum stress were 12.47mm and 113.8Mpa, respectively.

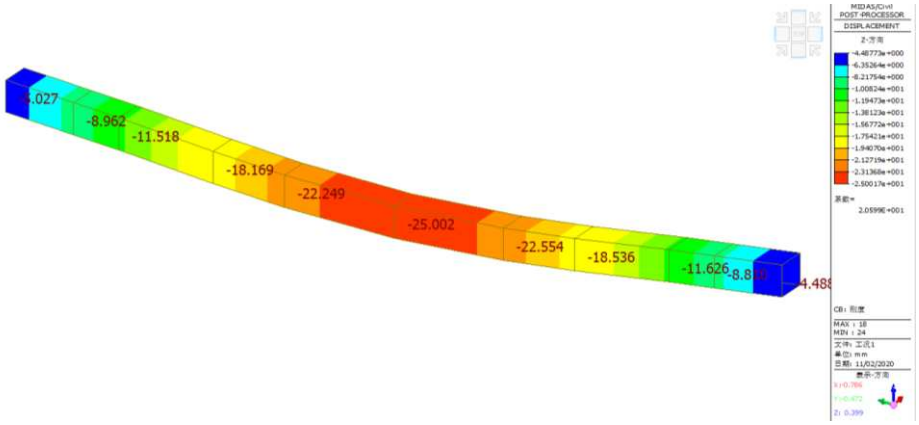

Figure 22. Structural distortion nephogram of front upper crossbeam under condition 1.

Preprints (www.preprints.org) | NOT PEER-REVIEWED | Posted: 26 July 2023 doi:10.20944/preprints202307.1758.v1

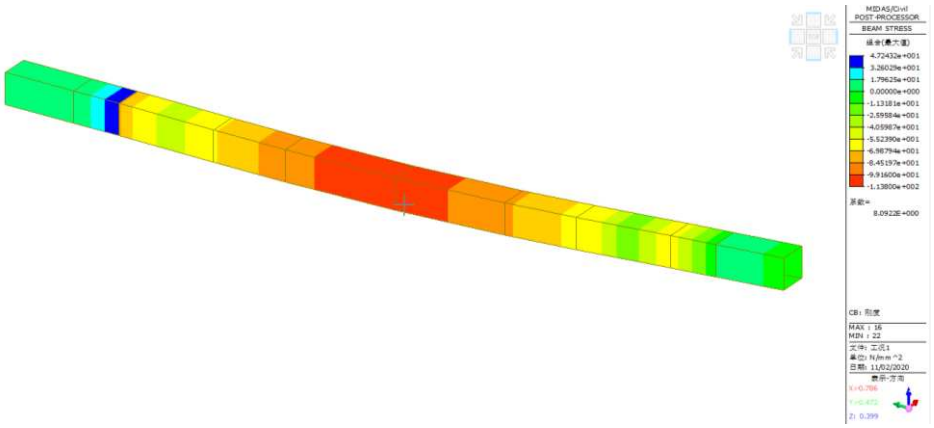

Figure 23. Stress nephogram of front upper crossbeam structure under condition 1.

3. Bottom Basket

The bottom basket provided the bearing for the formwork and concrete pouring. According to the finite element analysis results of Figures 24 and 25, the maximum distortion of the bottom basket structure occurred in the suspender position in the middle of the front lower beam suspension, which was 28.65mm. Due to the reference system, the actual maximum distortion of the front lower beam was 16.12mm. In addition, the maximum stress occurred in the middle of the bottom longitudinal beam of the outermost web, which was 72.8Mpa. The maximum distortion and stress of the bottom basket structure met the engineering design requirements.

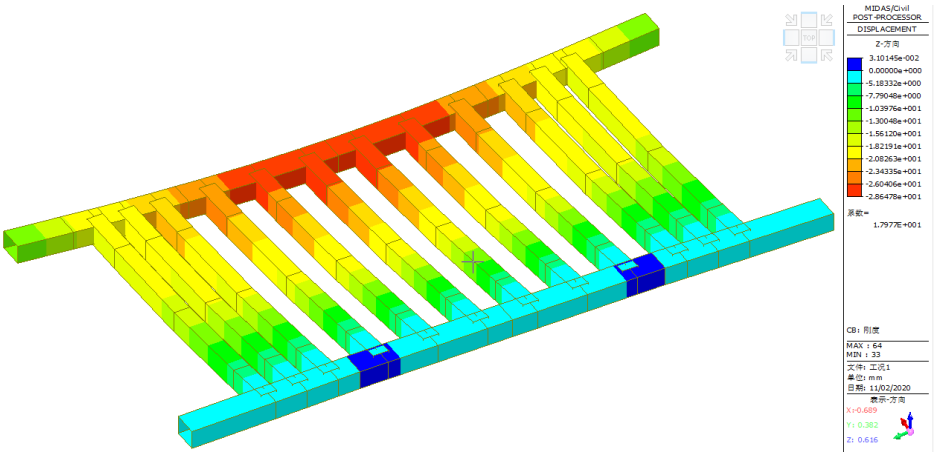

Figure 24. Cloud diagram of structural distortion of bottom basket under condition 1.

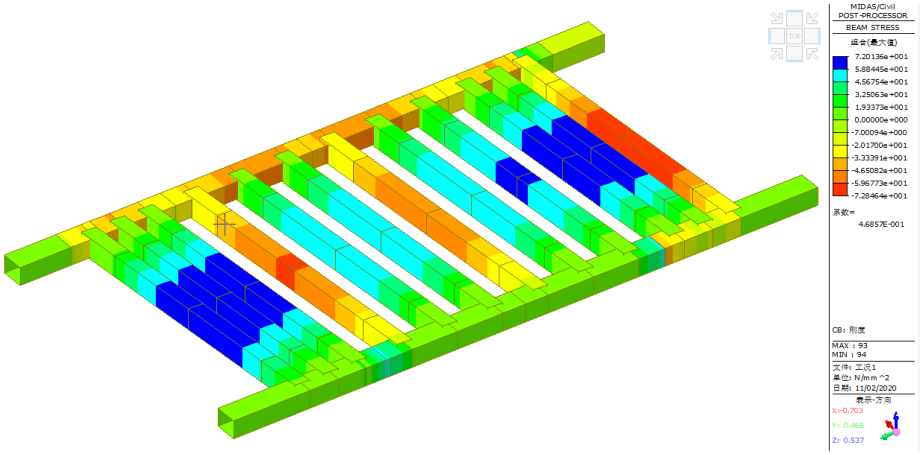

Preprints (www.preprints.org) | NOT PEER-REVIEWED | Posted: 26 July 2023 doi:10.20944/preprints202307.1758.v1

Figure 25. Stress nephogram of bottom basket structure under condition 1.

4. Hanger Rod

The five hanger rods of the project were connected to the front upper beam and the front lower beam of the bottom basket. And the material was PSB785Φ32 finish rolled deformed steel bar. In order to ensure the engineering quality, each suspender can meet the design requirements. According to the finite element analysis results in Figures 26 and 27, the maximum distortion of No.5 hanger rod at the front lower beam position was 16.11mm, and the maximum stress at both ends of No. 1 hanger rod was 407.07Mpa, which was less than the allowable stress of 650Mpa. The information about suspender distortion and stress was shown in Table 6.

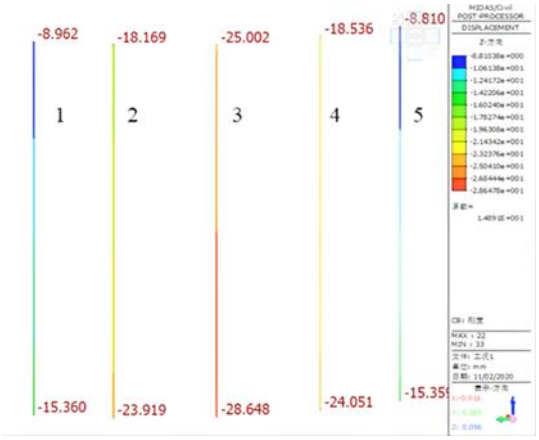

Figure 26. Nephogram of suspender distortion under condition 1.

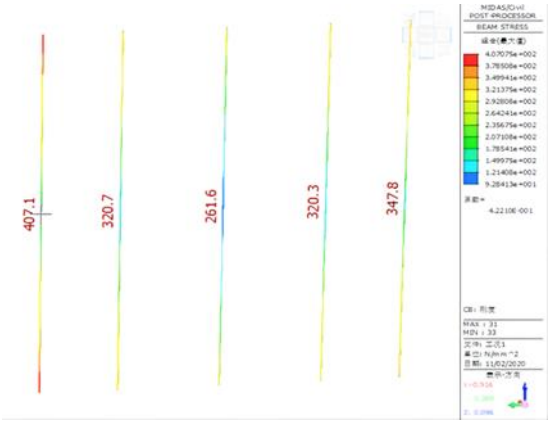

Figure 27. Nephogram of suspender stress under condition 1.

Table 6. Distortion and stress information of suspender in condition 1.

Suspender name	Max distortion [mm]	Max stress [Mpa]	Allowable stress[Mpa]
1	2.83	470.1	650
2	11.39	320.7	650
3	16.11	261.6	650
4	11.52	320.3	650
5	2.83	347.8	650

B. Analysis on Mechanical Performance of the Hanging Basket under Condition 2

In condition 2, the hanging basket walked to the end of the newly poured section, and it did not carry concrete, so the load it received was relatively small, but because it was in the last walking state,

Preprints (www.preprints.org) | NOT PEER-REVIEWED | Posted: 26 July 2023 doi:10.20944/preprints202307.1758.v1

the telescopic sleeve of the lower chord of its main truss was fully extended. Therefore, the force of the structure still needed to be verified by simulation. After the hanging basket model of condition 2 was established in Midas/Civil software, load and boundary conditions were added. The overall distortion cloud map and stress cloud map of the structure of condition 2 were shown in Figures 28 and 29, respectively. It can be seen from Figure 28 that the maximum distortion of the structure of the hanging basket under working condition 2 was at the front end point of the right main truss, and its value was 10.70mm, which was less than 13.25mm of the length of the rod.

It can be seen from Figure 29 that the maximum stress of the structure of the hanging basket of working condition 2 was 137.1Mpa, which occurred at the position of the lower chord of the right main truss; larger stress was generated, but the stress on the structure was less than the allowable stress of Q235 steel 175Mpa, which met the design requirements of the project. The main components of the hanging basket in working condition 2 were analyzed below.

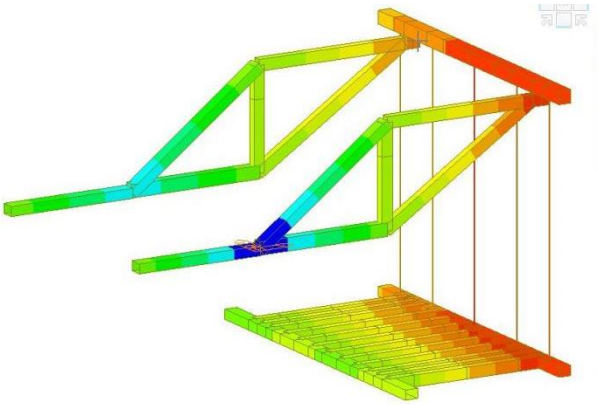

Figure 28. Cloud diagram of Z-direction distortion of overall structure of hanging basket under condition 2.

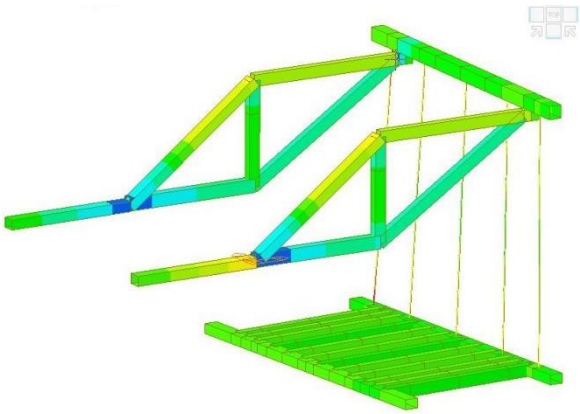

Figure 29. Cloud diagram of overall structural stress of hanging basket under working condition 2.

1. Main truss

Different from condition 1, in addition to the original five members (upper and lower chords, vertical web members, tension sloping web members and compression sloping web members) of the main truss, the telescopic beam (AE) in the lower chord extended out. Due to the movement requirements, the rear anchor point untied the two flat load beams, leaving only one anchor for anchorage, resulting in a change in the load-bearing mode of the hanging basket. The material of each component was Q235. From the finite element analysis results of Figures 30 and 31, it can be known that the maximum distortion of the front end point of the main truss was 10.70mm, and the maximum stress was 137.1Mpa.

Preprints (www.preprints.org) | NOT PEER-REVIEWED | Posted: 26 July 2023 doi:10.20944/preprints202307.1758.v1

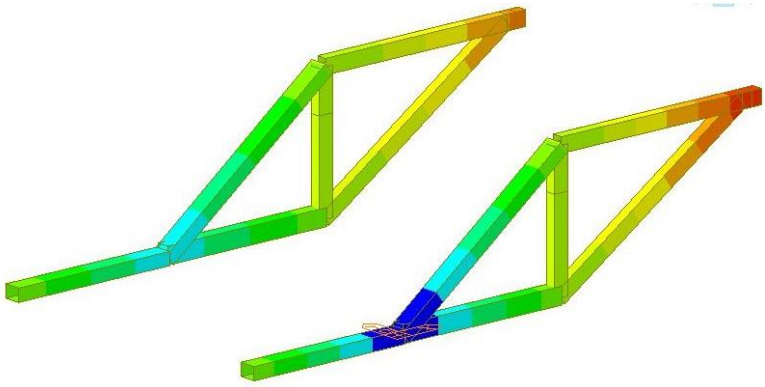

Figure 30. Cloud diagram of main truss structure distortion under condition 2.

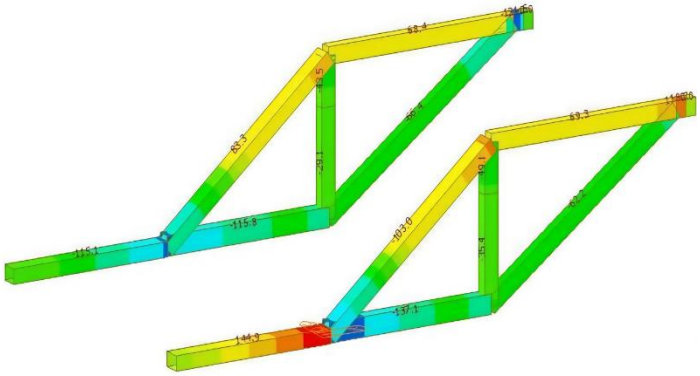

Figure 31. Cloud diagram of main truss structure distortion under working condition 2.

The maximum stress and distortion analysis of each member of the main truss was shown in Table 7. It can be seen from Table 7 that each member of the main truss meets the design requirements of the project.

Table 7. Analysis of the members of main truss under condition 2.

Member name	Maximum stress	Maximum vertical distortion/mm	Allowable stress/Mpa	Allowable distortion/mm
AB	137.1	16.9	175	11.75
CD	118.7	9.9	175	13.25
BD	49.1	0.12	175	9.00
AD	103.0	7.0	175	14.91
BC	62.2	9.7	175	15.25
AE	114.9	7.1	175	11.25

2. Front upper beam

In condition 2, the distortion and stress cloud diagrams of the front upper beam were shown in Figures 32 and 33. From the figures, the maximum distortion of the front upper beam occurred at the right end of the beam, and its real distortion was 12.96mm. The maximum stress on the upper beam was 56.7Mpa.

 doi:10.20944/preprints202307.1758.v1

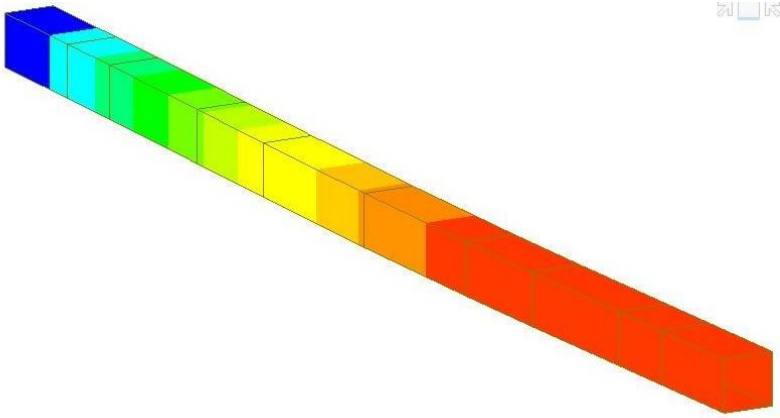

Figure 32. Cloud diagram of structural distortion of front upper beam under working condition 2.

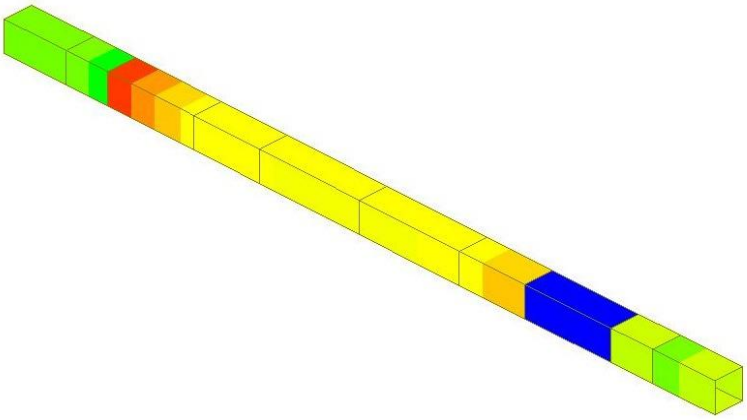

Figure 33. Nephogram of structural distortion of the front upper beam under condition 2.

3. Bottom basket

From the finite element analysis results of Figures 34 and 35, it can be seen that the maximum distortion generated in the bottom basket structure was 12.54mm, which was located at the right end of the front lower beam, and the maximum stress was 93.36Mpa, which occurred in the rear lower beam. The structure of each part of the bottom basket composed of the lower bottom longitudinal beam of the web plate, the lower bottom longitudinal beam of the bottom plate and the front and rear lower transverse beams met the the construction requirements.

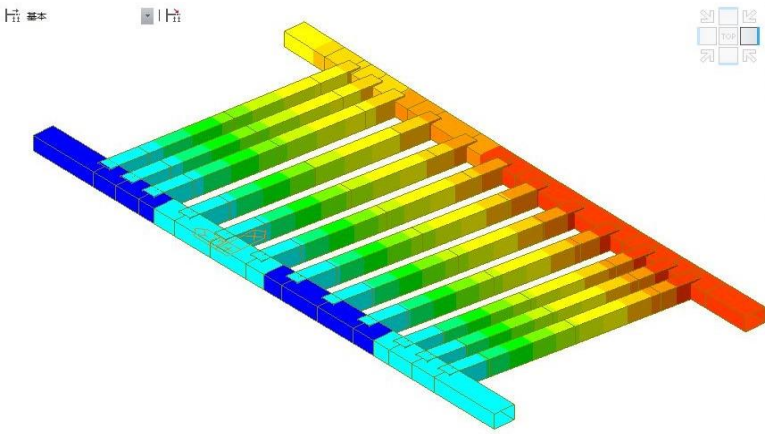

Preprints (www.preprints.org) | NOT PEER-REVIEWED | Posted: 26 July 2023 doi:10.20944/preprints202307.1758.v1

Figure 34. Cloud diagram of structural distortion of bottom basket under working condition 2.

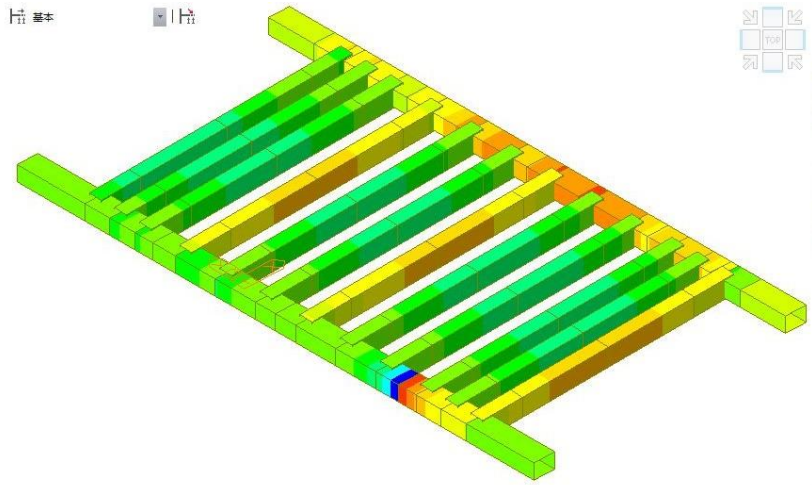

Figure 35. Cloud diagram of structural distortion of bottom basket under working condition 2.

4. Suspender

The finite element analysis results of the suspender in working condition 2 were shown in Figures 36 and 37, respectively. It can be seen from the figure that the maximum distortion of the structure occurred in the No. 5 suspender with a value of 23.18mm, and the maximum stress occurred in the No.1 suspender with a value of 295.4Mpa, which was less than the allowable stress of 650Mpa. The structural the construction requirements, the distortion value and the stress of the suspender were shown in Table 8.

Table 8. Suspender distortion and stress information under condition 2.

Suspender name	Maximum distortion/mm	Maximum stress/Mpa	Allowable stress/Mpa
1	17.13	295.4	650
2	19.37	218.8	650
3	21.76	260.1	650
4	22.94	162.3	650
5	23.18	167.9	650

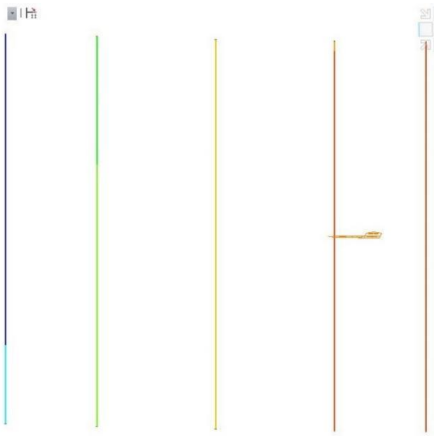

Figure 36. Cloud diagram of suspender structure distortion under working condition 2.

Preprints (www.preprints.org) | NOT PEER-REVIEWED | Posted: 26 July 2023 doi:10.20944/preprints202307.1758.v1

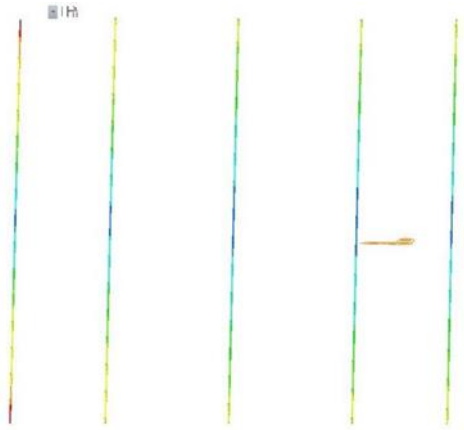

Figure 37. Cloud diagram of suspenderr structure distortion under working condition 2.

C. Analysis on Mechanical Performance of the Hanging Basket under Condition 3

In order to analyse the mechanical performance of condition 3, it was indispensable to calculate its anti-overturning performance. In condition 3, the hanging basket was in the walking state, where the wind direction was vertically downward. According to Equation (2), Wd represented wind load, γa.=1.25kg/m3 represented air density, Vw=13.6m/s represented wind speed. According to Equations (3) and (4), the dead weight load of the main truss was G1=63000kg; Dead weight load of the formwork was G2=63000kg. In addition, the arms of force X, X1 and X2 were 5000mm, 1000mm and 2500mm respectively. In addition, the acceleration of gravity was g.

$$W_{\mathrm{d}} = \frac{\gamma_a V_w}{2g} \tag{2}$$

$$M_{Q1} = G_1 g X_1 \tag{3}$$

$$M_{Q2} = G_2 g X_2 \tag{4}$$

Therefore, the total overturning moment of the hanging basket equipment was MQ1, MQ2 and MQ3, which added up to 1.36×106 N·M; The anti-tipping moment of the equipment mainly came from the two rear walking trolleys. As the ultimate bearing capacity of a single trolley was 3.5×105N. And the stabilizing moment generated by the trolley was q5=1kN/m, so the anti-overturning coefficient of the hanging basket was 2.57 (more than 2).

Consequently, the overall anti-overturning performance of the hanging basket in walking condition met the operating requirements. Therefore, the overturning moment generated by the wind load was MQ3=WdX. The overturning moment generated by the dead weight of the main truss and the overturning moment generated by the dead weight of the formwork system were shown in Equations (3) and (4) respectively.

2.4. Verification of Key Components and Analysis of the Weak Structures

In this chapter, the distortion and stress of each part of the hanging basket structure were calculated, and compared with the results of the previous chapter. The applicability of the finite element simulation method was verified. Ultimately, the paper put forward some suggestions of optimization of the distortion and stress of the main working conditions.

Preprints (www.preprints.org) | NOT PEER-REVIEWED | Posted: 26 July 2023 doi:10.20944/preprints202307.1758.v1

2.4.1. Member Calculation

The 9# block length was 4.5m, and the segment volume was 79.6m3. According to the stress mode of the hanging basket mentioned above, the layout of the front lower beam and bottom longitudinal beam of the hanging basket was shown in Figure 38. In the calculation of this section, the concrete bulk density was γ=2.6t/m3, the overload coefficient of concrete the construction was k1=1.05, the partial load coefficient was k2=1.2, and L' was the length of the current calculation beam section.

A. Bottom Longitudinal Beam of Web

Take the bottom longitudinal beam as an example to calculate its deflection. The bottom longitudinal beam under the web and the bottom longitudinal beam under the bottom plate was calculated as simply supported beams. Because the bearing position and bearing capacity were different, they were treated separately for the calculation. If the section area of box girder web was s1=4.12m2, the load q1 of the longitudinal beam under the 9# box girder web was shown in Equation (5).

$$q_1 = s_1 \gamma k_1 k_2 = 135\text{kN/m} \tag{5}$$

The load of the external operation platform was q2=2.5kN/m2, the dead weight of each longitudinal beam was q3=0.33kN/m, and the weight load of the upper bottom formwork of each longitudinal beam was q4=0.34kN/m. The longitudinal beam under the web was calculated as a simply supported beam, and the calculation diagram was shown in Figure 39. There were two longitudinal beams under the 9# segment web, but only one was considered in the calculation, so the actual load qwb of the longitudinal beam under the web was shown in Equation (6).

$$q_{wb} = \frac{q_1}{2} + q_3 + q_4 = 68.52\text{N/mm} \tag{6}$$

The reaction force of the two fulcrums of the bottom longitudinal beam under the web was 154.13kN, the deflection of the bottom longitudinal beam under the web was shown in Figure 40, and the maximum deflection of the structure was 9.7mm (less than 15.25mm).

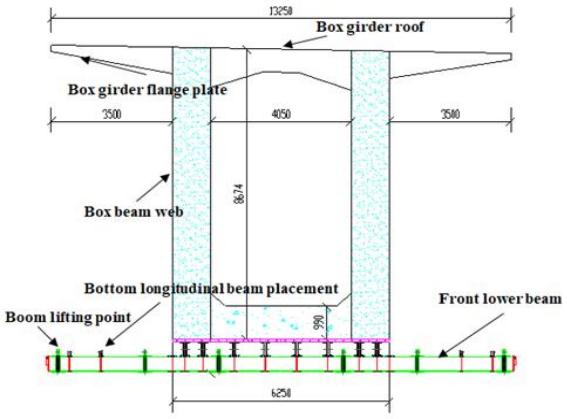

Figure 38. Front lower beam and bottom longitudinal beam.

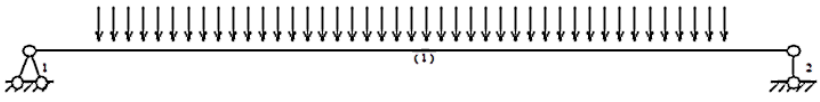

Figure 39. Calculation stress diagram of bottom longitudinal beam under Web.

Preprints (www.preprints.org) | NOT PEER-REVIEWED | Posted: 26 July 2023 doi:10.20944/preprints202307.1758.v1

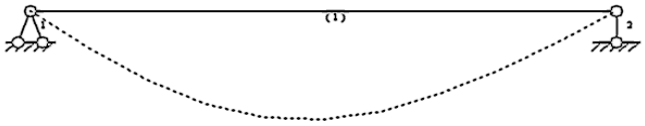

Figure 40. Deflection diagram of bottom longitudinal beam under Web.

B. Bottom Longitudinal Beam under Bottom Plate

The longitudinal beam under the box girder bottom plate bore the load of the box girder bottom plate, the cross-sectional area of the box girder bottom plate was s2=3.12m2. And the load of the longitudinal beam under the box girder bottom plate was shown in Equation (7). The weight of the upper bottom formwork of each longitudinal beam was q5=1kN/m, and the bottom longitudinal beam of the bottom plate was calculated as a simply supported beam. The calculation diagram was shown in Figure 41, and the actual load qbb of the bottom longitudinal beam of the bottom plate was shown in Equation (8). The reaction force of the two fulcrums of the bottom longitudinal beam under the bottom plate was 78.32kN, the deflection of the bottom longitudinal beam under the bottom plate was shown in Figure 42, and the maximum deflection of the structure was 13.5mm (less than 15.25mm).

$$q_4 = s_2 \gamma k_1 k_2 = 102.2\text{kN/m} \tag{7}$$

$$q_{bb} = \frac{q_4}{2} + q_3 + q_5 = 34.81\text{N/mm} \tag{8}$$

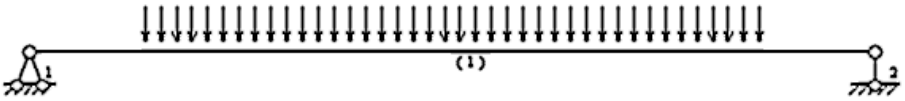

Figure 41. Calculation stress diagram of bottom longitudinal beam under bottom plate.

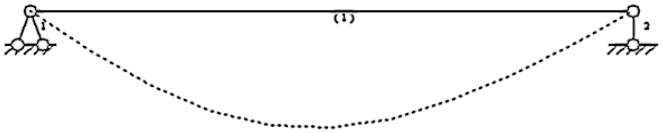

Figure 42. Deflection diagram of bottom longitudinal beam under bottom plate.

2.4.2. Analysis of the Weak Structure

In condition 1, the main components of the hanging basket structure were decomposed into a single element, the axial force, stress and strain of some main components were obtained. By comparing the calculation results with the calculation results of the previous chapter, it was found that the finite element analysis results were not much different from the theoretical calculation results. Therefore, it was reliable to calculate the stress of the hanging basket of MIDAS/Civil. In order to optimize the hanging basket more pertinently, the results obtained in the analysis and calculation were redundant with the allowable stress of the bar. The summary of the finite element calculation results and the allowable values of the members of the equipment were shown in Table 9. It can be seen from Table 9 that in the main structure of the hanging basket, the performance redundancy of the distortion of the main truss CD bar, the bottom longitudinal beam under the floor, the front lower cross beam and the stress of the main truss BC bar were less than 30%, while the performance redundancy of other bars was more than 30%. And all member materials were Q235. For this reason, the rigidity of the CD bar of the main truss, the lower bottom stringer of bottom plate, the front lower beam, and the strength of the BC bar of the main truss should be focused in the subsequent researches.

Preprints (www.preprints.org) | NOT PEER-REVIEWED | Posted: 26 July 2023 doi:10.20944/preprints202307.1758.v1

Meanwhile, given that most bars had high performance redundancy, the amount of carried concrete can be increased to extend the casting segment.

Table 9. Comparison of finite element calculation results and allowable values of members.

Member		Finite element analysis results		Allowable value		Performance redundancy	
		Stress [Mpa]	Distortion [mm]	Stress [Mpa]	Distortion [mm]	Stress [%]	Distortion [%]
Main Trusses	AB	92.6	0.21	175	11.75	47.09	98.21
	AD	103.9	0.60	175	14.91	40.63	95.98
	BC	134.2	10.33	175	15.25	23.31	32.26
	BD	55.0	0.41	175	9.00	68.57	95.44
	CD	119.7	12.53	175	13.25	31.60	5.43
Front upper crossbeam		113.8	12.47	175	18.13	34.97	31.22
Bottom longitudinal beam	Under the Web	71.32	9.05	175	15.25	59.25	40.66
	Under the floor	57.99	13.67	175	15.25	66.86	10.36
Lower cross beam	Front lower beam	52.93	16.12	175	18.00	69.75	10.44
	Lower rear beam	48.59	9.80	175	18.00	72.23	45.56

3. Results

This chapter first took the main truss structure as the research object, carrying on the simulation analysis of changing the front elevation angle of the main truss and the beam structure respectively. And it was found the most suitable main truss structure of the corresponding project, prolonged the pouring beam section, increased the carrying capacity of single walking concrete, made the improved structure more suitable for the current project, and further enhanced the engineering efficiency.

3.1. Main Truss Optimization

A. Front elevation of Main Truss

The schematic diagram of the front elevation angle of the main truss of the hanging basket was shown in Figure 43, and the range of the front elevation angle can be taken as 0-35 degrees. In this paper, the initial front elevation was 35°, and the front elevation was gradually reduced to 5 degrees when the horizontal distance between the upper end of the main truss and the web member was fixed. According to the simulation results, the most suitable front elevation value was analyzed. And the range of the front elevation angle can be taken as 0-35 degrees. In this paper, the initial front elevation was 35°, and the front elevation was gradually reduced to 5 degrees when the horizontal distance between the upper end of the main truss and the web member was fixed. According to the simulation results, the most suitable front elevation value was analysed.

Preprints (www.preprints.org) | NOT PEER-REVIEWED | Posted: 26 July 2023 doi:10.20944/preprints202307.1758.v1

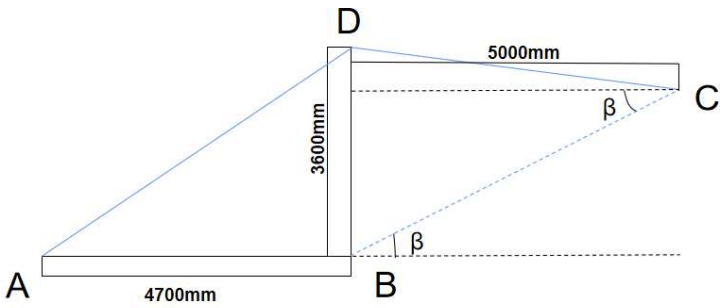

Figure 43. Front elevation of main truss.

The front angle of elevation of each simulation model was 5° lower than that of the previous model. Except the model with a front angle of elevation of 35°, 6 additional groups of simulation models were established for the analysis of changes in bar length and steel consumption caused by the changes of the angle, as shown in Table 10 and Figure 44. According to the analysis, relying on the previous finite element calculation, the load was applied. In the most unfavorable condition 1, at the point C, the single main truss of was subjected to the pressure of 399.32t, which was respectively applied to the newly established six models. And the changes of stress in various bars were shown in Figure 45. Because the z-direction distortions of the BC and CD bars of the main truss were relatively large, the other three bars can be ignored.

Table 10. Model parameters for changing front elevation angle.

Front elevation angle	35°	30°	25°	20°	15°	10°	5°
BC+BD Pole length[m]	11.161	10.824	10.675	10.628	10.664	10.768	10.935
BC+BD Rod steel amount[kg]	1421.5	1378.5	1359.6	1353.6	1358.1	1371.4	1392.7

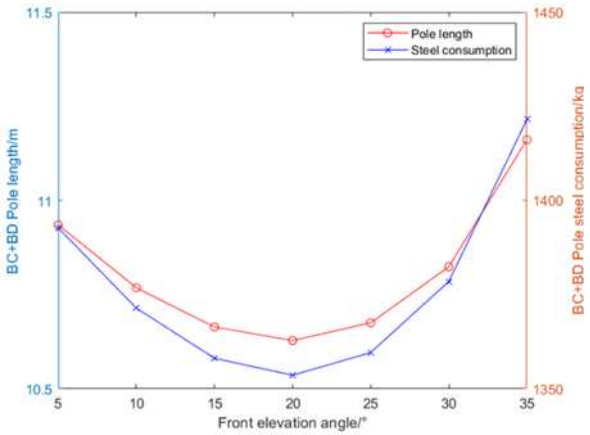

Figure 44. Schematic diagram of model parameters change caused by the change of front elevation angle.

Preprints (www.preprints.org) | NOT PEER-REVIEWED | Posted: 26 July 2023 doi:10.20944/preprints202307.1758.v1

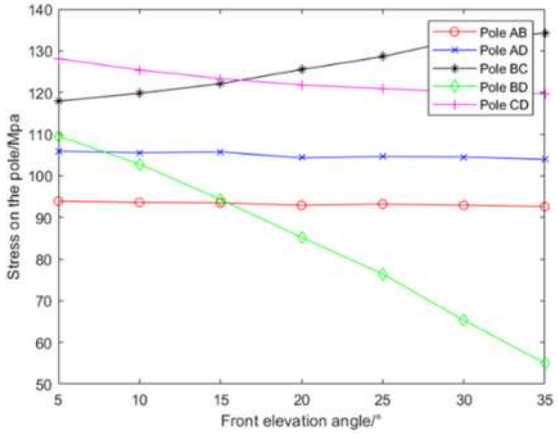

Figure 45. Stress variation of model member caused by change of front elevation angle.

The comparison of z-direction distortions in BC and CD bars was shown in Figure 46. It can be seen from the analysis of Figure 44 that when the horizontal distance between the upper end of the main truss and the web member was fixed, the front elevation angle of the main truss was reduced, and the steel consumption of the hanging basket was changed. In the range of 35-5° front elevation, the sum of BC and BD pole length was first decreased and then increased. When the front elevation was 20°, the length of BC + BD pole was the smallest, which was 10.628m. And the steel consumption was the least, which was 1353.6kg.

It can be seen from the analysis of Figure 45 that the stress changes of each member were different, and the stress changes of AB and AD poles were not obvious and can be ignored. In comparison, stress of BC、BD and CD bars witnesses changed significantly, in which the stress of BC bar was decreased with the reduction of the front angle of elevation and the deceleration gradually eased off. As the BD bar belonged to the vertical belly pole, its stress was drastically increased with the reduction of the front angle of elevation. The stress of CD bar was increased with the reduction of the front angle of elevation, and the deceleration gradually eased off. As can be seen from the analysis of Figure 46, the distortions of BC and CD bars with large vertical distortion of the main truss were first decreased and then increased to the reduction of the front angle of elevation. It can be observed that the changes were relatively small and the max distortion was still within the allowable distortion in the bar.

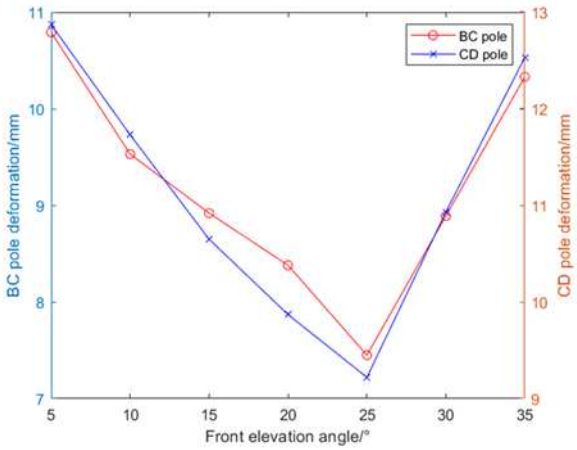

Figure 46. Distortion of important members of the model.

Based on the above simulation results and data, the optimal structure was selected when the front elevation angle was 20° and the steel consumption of BC + BD was 1353.6kg. The stress of AB, AD, BC, BD and CD were 92.9, 104.3, 125.5, 85.2 and 121.8Mpa respectively. The vertical distortion

of BC and CD poles were 8.38mm and 9.87mm separately. The structure of the front elevation angle was shown in Figure 47, and the structure was substituted into the subsequent research for analysis.

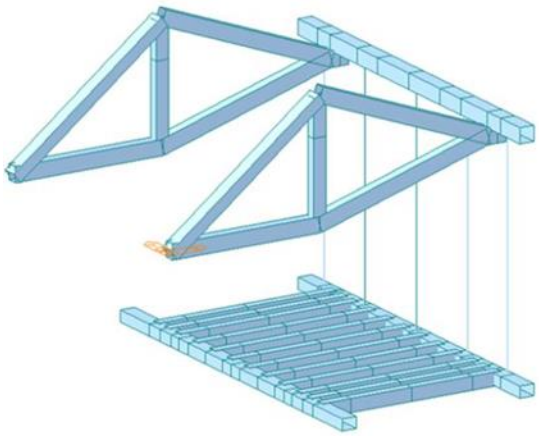

Figure 47. Hanging basket structure with a front elevation angle.

B. Main Truss Beam structure

In the previous calculation, it was found that the mechanical performance of most members of the main truss had great redundancy. Therefore, in addition to optimizing the elevation angle and the mentioned extension of the pouring section, the beam structure can be changed, that was, the beam section can be changed to reduce the steel consumption of the equipment to improve the engineering efficiency. In the initial simulation calculation, each member of the main truss was made of steel, and the vertical web member (BD) of the main truss was □350×250×12mm, the upper chord (CD), lower chord (AB) and compression diagonal web (BC) of the main truss were □400×300×12mm, the tension diagonal web member (AD) of the main truss was □420×300×12mm. Since it was found that the rigidity of CD pole and the strength of BC pole were close to the allowable stress in the calculation, only AB, AD and BD poles were optimized while maintaining the structure with the elevation angle of 20° before the upper section, keeping the length of BC and CD unchanged. The information of optimized poles was shown in Table 11. It can be seen from Table 11 that after optimization, the weight of AB, ad and BD poles was reduced by 14.976kg, and the steel consumption was reduced by 29.952kg because the hanging basket structure was symmetrical.

Table 11. Comparison table of optimized main truss member information.

	Original dimension of pole /mm	Optimized pole size /mm	Reduced steel consumption /kg
AB pole	□400×300×12mm	□380×280×12mm	3.744
AD pole	□420×300×12mm	□400×280×12mm	7.488
BD pole	□350×250×12mm	□330×230×12mm	3.744

3.2. Optimization of Pouring Section

According to the previous calculation, it was found that the stiffness of the main truss except CD member and the strength of BC member had greater performance redundancy. In the actual the construction, the single span was 100m, the construction of the hanging basket was required to be divided into 24 segments for symmetrical casting, and the lengths of the segments were 3.5m, 4m, and 4.5m respectively. In other words, the hanging basket needed to walk for 12 times, of which there were two segments for 3.5m. In addition, four segments for 4m and six segments for 4.5m, which served as the heaviest segment weighing at 206.96t. In this section, the casting segment was extended by 0.5m, while the heaviest segment was increased to 5m in length and to 229.96t in weight. The load value was applied to the optimal model established and affirmed in the section of 5.1, so the distortion and stress nephogram of the hanging basket were obtained, as shown in Figures 48 and 49.

Preprints (www.preprints.org) | NOT PEER-REVIEWED | Posted: 26 July 2023 doi:10.20944/preprints202307.1758.v1

It can be seen from Figure 48 that the vertical distortion of 13.14mm occurred at the upper end of the main truss, which was less than 1/400 of the length of the pole(13.27mm); the vertical displacement of 29.55mm occurred in the middle of the front upper beam, which was less than 1/400 of the length of the pole(30mm) due to the reference system; In the bottom basket structure, the vertical displacement of 33.09mm occurred in the middle of the front lower beam, which was due to the reference system. According to different reference systems, the actual distortion of the pole was 19.95mm; the distortion of the lower part of No. 3 suspender was 19.95mm. The distortion of the structure met the design requirements. As can be seen from Figure 49, except the suspender, the maximum beam unit internal force generated by the whole structure was 161.19Mpa, which occurred at the junction of the front upper beam and the main truss. The structural stress was less than the allowable stress 175Mpa of Q235 steel $[\sigma^{a}_{Q235}]=175\text{Mpa}$. The maximum stress at both ends of No.1 suspender was 406.17Mpa, which was less than the allowable stress 650Mpa of the finish rolled rebar and met the design requirements of the project.

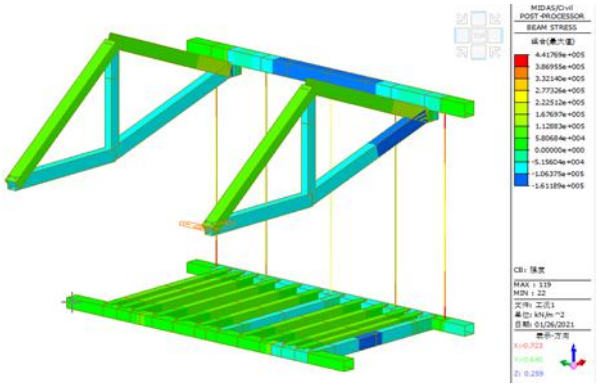

Figure 48. Z-direction distortion nephogram of overall optimized structure of hanging basket for extended casting segment.

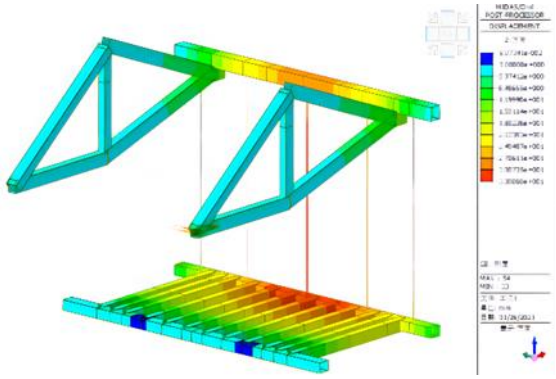

Figure 49. Stress nephogram of overall optimization structure of hanging basket for extended casting segment .

In this section, first of all, the simulation results showed that when the front elevation angle was 20 °, the steel consumption of the main truss was the least, and under the condition of improving the front elevation angle, the optimization of the beam structure can reduce the steel consumption of the two main trusses by 29.952kg; Secondly, when the optimized main truss structure was determined, the pouring section was extended by 0.5m. After the finite element simulation of the new the construction scheme, it was found that the stress of the hanging basket structure after the extension of the pouring section still met the engineering requirements. The maximum deformation of the main truss structure was 13.14mm and the maximum stress was 161.19Mpa. The optimization of structure and the construction saved engineering resources and costs.

 doi:10.20944/preprints202307.1758.v1

4. Discussion

The traditional hanging basket walking mechanism was to lay steel rails on the box girder working panels, which were fixed by front and rear supports and prestressed steel bars. The height of the steel rails was higher, which was increased the overall center of gravity of the equipment and raised the overturning of the hanging basket during the construction. In addition, the walking track was long and heavy, and the process of paving and dismantling was complicated, which limited the improvement of the efficiency of bridge the construction. Relying on the Tianjin Haihe Bridge, this paper designed a novel rhombus traveling track of hanging basket, which had higher tensile strength, higher compressive strength and better impact resistance than traditional rails. The design and analysis of the force state of the rhombus hanging basket running under different working conditions, and the finite element simulation and calculation were carried out; based on the simulation and calculation results, the suitable hanging basket transformation for the project was proposed and verified. The scheme optimized the structure of the hanging basket components, reduced weight and saved costs, shortened the the construction period, and improved the construction efficiency.

Using Midas/Civil software, the mechanical properties of the rhombus hanging basket under three working conditions, fully loaded and unloaded, were analyzed. In working condition 1, the maximum beam unit internal force of 149.69Mpa occurred at the joint between the front upper beam and the main truss, which was less than the allowable stress of Q235 steel 175Mpa. In working condition 2，the maximum stress occurred in the No.1 suspender with a value of 295.4Mpa, which was less than the allowable stress of 650Mpa. In working condition 3, the anti-overturning safety factor of the hanging basket was 2.5 to meet the requirements, and the strength and distortion of the walking mechanism were within the specified range; the key components were calculated and compared with the finite element calculation, and it was found that the finite element calculation was reliable and the structure performance was 30% left and right redundancy. In order to further improve the utilization efficiency of the suspended pouring basket, the main truss and the pouring stage were optimized. It was found that when the front elevation angle of the main truss was 20°, the steel consumption was the least, the member stress was small, and the stress of each member was relatively uniform and small vertical distortion; when the pouring section was extended by 0.5m, the heaviest section was extended to 5m, and the working condition when the weight was increased to 229.96t, the working condition still met the requirements. The research results of this paper can provide references to the structural optimization and improvement of the rhombus hanging basket and similar cantilever the construction projects.

Author Contributions: Yuping Ouyang management and coordination responsibility for the research activity planning and execution. Jiarui Huang and Kaifang Song designed the experiments and Jiarui Huang carried them out. Kaifang Song used the civil software titled and performed the simulations. Jiarui Huang prepared the manuscript with contributions from all co-authors.

Funding: This paper was supported by Key research and development Project of Jiangxi Province: Research and application of Key Technologies of intelligent Management System of hilly and mountainous orchard Transport Equipment based on "Internet +" (20202BBF63016); Key research and application of Key Technologies of efficient intelligent Freight system of mountainous orchard (20212BBF63041). The authors are grateful for the support.

Data Availability: The data used to support the findings of this study are included within the article.

Conflicts of Interest: The authors declare that they have no conflicts of interest.

Nomenclature

a_{cU}	The impact strength of the specimen(kJ/m$^{2)}$
h_{cU}	The thickness of the specimen (mm)
E_{cU}	The energy absorbed by the measured pattern (J)
b_{cU}	The width of the specimen (mm)
W_d	The wind load
γ_a	The air density(kg/m$^{3)}$

 doi:10.20944/preprints202307.1758.v1

V_w	The wind speed (m/s)
g	The acceleration of gravity
M_Q	The overturning moment of the hanging basket equipment(N·m)
G	The dead weight load(kg)
X	The arm of force(mm)
q	The load of structure
s	The cross-sectional area of structure(m^2)
γ	The concrete bulk density($t/m^{3)}$
k	The load coefficient

References

1. Hyo, G. K. and Je, K.S.: Span ratios in bridges constructed using a balanced cantilever method , The construction and Building Materials, vol.18, no.10, pp.767-779, doi:10.1016/j.conbuildmat.2004.04.022, 2004.
2. Won, J. H., Cho, K. I., Yoon, J. H. et al.,: Innovative key-segment closing method using thermal pre-stressing technique for partially earth-anchored cable-stayed bridges, Advances in Structural Engineering, vol.11, no.5, pp.549–564, doi:10.1260/136943308786412041, 2008.
3. Liu, Z. W., Zhou, J.T., Ma, H. et al.,: Key technology of hanging basket suspension casting construction of yelanghu super large bridge, World bridge, vol.47, no.5, pp.22-26, doi:10.3969/j.issn.1671-7767.2019.05.005, 2019.
4. Zhao, X. J., He, S. H., Li, Y. et al.,: Simulation analysis of the construction process of front fulcrum han-ging basket of cable-stayed bridge, Journal of Shenzhen University(Science and Engineering Edition),vol.34, no.2, pp. 138-146, doi:10.3724/SP.J.1249.2017.02138, 2017.
5. Mashal, M. and Palermo, A.: Low-damage seismic design for accelerated bridge the construction, Journal of Bridge Engineering, vol.24, no.7, Article ID 04019066, doi:10.1061/(asce)be.1943-5592.0001406, 2019.
6. Li, Q. F., Qian, H. J., Pei, J. J. et al.,: Safety risk analysis of bridge rhombic hanging basket construction based on WBS-RBS and rough set theory ,Materials Science and Engineering, vol.780, no.7,pp.072033,doi:10.1088/1757-899x/780/7/072033, 2020.
7. Li, L.: Research on key technology of suspension casting the construction of long-span continuous beam bridge, M.S. dissertation, Mar. Elect. China., Anhui University of technology, Huainan City, Anhui Province, China, doi:10.7666/d.Y3396284, 2018.
8. Gao, J.: Guyed Traveler Composite of the Central Cable Plane PC Cable-stayed Bridge with Wide Girder Application Technology, M.S. dissertation, Mar. Elect. China., Changan Univ., Xi'an City, Sh-aanxi Province, China, doi:10.7666/d.D01114161, 2016.
9. Chen, L. Y.: Using Midas software to design the main truss of triangular hanging basket for contin-uous beam the construction, National Defense Transportation Engineering and technology, vol.11, no.3,pp.75-77, doi:10.3969/j.issn.1672-3953.2013.03.021, 2013.
10. An, D. Q.: Research on Structural Analysis and Optimization of Rhombus Hanging Basket for the Up and Down Double Chamber Continuous Rigid-framed Aqueduct, M.S. dissertation, Mar. Elect. China., Zhengzhou Univ., Zhengzhou City, Henan Province, China, doi:CNKI:CDMD:2.1018.088893, 2018.
11. Gu, S. F.: Research on Key The construction Technique of Long-span and Broad-width PC Box GirderBridge with Corrugated Steel Webs, Railway The construction Technology, vol.12, no.12, pp.49-53, doi:10.13468/j.cnki.chw.2019.11.033, 2019.
12. He, J., Li, X., Li, X. et al.,: A novel asynchronous-pouring-the construction technology for prestressed concrete box girder bridges with corrugated steel webs, Structures, vol.27, pp.1940-1950, doi:10.1016/j.istruc.2020.07.077, 2020.
13. Zhou, M., Liu, Y. Y. and Wang, K.: New Asynchronous-Pouring Rapid-The construction Method for Long-Span Prestressed Concrete Box Girder Bridges with Corrugated Steel Webs, Journal of The construction Engineering and Management, vol.146, no.2, Article ID 05019021, doi:10.1061/(asce)co.1943-7862.0001770, 2020.
14. Xie, W., Zhao, T. and Tang, J.:Arch first and beam later: arch-rib integral installation the constructiontechnology for large-span tied-arch bridge, Journal of The construction Engineering and Management,vol.143, no.8, Article ID 04017059, doi:10.1061/(asce)co.1943-7862.0001356, 2017.
15. Somaini, D. and Furst, A.: The new bridge over the Saane: modern steel girder for the historic railwayviaduct, Stahlbau, vol.89, no.7, pp.622-627, doi:10.1002/stab.202000041, 2020.
16. Li, R. C., Gui T. J., Cong, W. W. et al.,: Synthesis and performance characterization of fluorin-econtaining silane coupling agent oligomer, Material Guide, vol.35, no.12, pp.2199-2206, doi:10.11896/cldb.19100208, 2021.
17. Kosobokov, M. D., Zubkov, M. O. and Levin, V. et al.,: Fluoroalkyl sulfides as photoredox-active coupling reagents for alkene difunctionalization, Chemical Communications, vol.56, no.66, pp.9453 -9456, doi:10.1039/d0cc04617e, 2020.
18. Ying, J. Q., Qiu, H. and Zhang, H. J.: Effect of Different Types of Toughening Agent on Properties of Polycarbonate, China Plastics, vol.34, no.7, pp.30-35, doi:10.19491/j.issn.1001-9278.2020.07.005, 2020.
19. Wolk, A., Rosenthal, M., Weiss, J. et al.,: Graphene oxide as flexibilizer for epoxy amine resins, Progress in Organic Coatings, vol.122, pp.280-289, doi:10.1016/j.porgcoat.2018.05.028, 2018.
20. Hu, Y., Weng, Z. and Qi, Y.: Self-curing triphenol A-based phthalonitrile resin precursor acts as a flexibilizer and curing agent for phthalonitrile resin, RSC advances, vol.8, no.57, pp.32899-32908, doi:10.1039/c8ra06926c, 2018.
21. Wu, X., Wu, T. T., Chen, W. Z. et al.,: Analysis of height difference between three trusses of a steel truss bridge during incremental launching, Stahlbau, vol.87, no.9, pp.910-922, doi:10.1002/stab.201810632,2018.

22. Zhou, X. H., Qin, F. J. and Di, J.: Continuity analysis method of plate-truss combined stiffening beam based on energy principle, Journal of China Highway, vol.27, no.6, pp.34-43, doi:10.19721/j.cnki.1001-7372.2014.06.005, 2014.